Block Copolymer Monolayer Structure Measured with Scanning Force Microscopy Moiré Patterns

Alexander Hexemer,[†] Gila E. Stein,[‡] Edward J. Kramer,[*,†,‡] and Sergei Magonov[§]

Department of Materials, University of California, Santa Barbara, California 93106; Department of Chemical Engineering, University of California, Santa Barbara, California 93106; and Veeco Metrology, Santa Barbara, California 93117

Received February 8, 2005; Revised Manuscript Received May 31, 2005

ABSTRACT: We demonstrate that an analytical model can be used to interpret moiré patterns in scanning force microscopy images of spherical domain block copolymer films, yielding grain orientations and a more than 10-fold increase in scan size without requiring a tedious empirical calibration. Moiré patterns are the product of interference between two overlapping regular gratings and are sensitive to the grating periodicity and alignment. We apply this technique to SFM of a monolayer of a spherical domain block copolymer, where the SFM scan lines act as a reference grating, and the close-packed rows of the block copolymer domains form the sample grating. The block copolymer grain orientation and size are calculated from the moiré patterns using an analytical model. The accuracy of the model is confirmed by directly imaging the block copolymer lattice with high-resolution SFM. Furthermore, we investigate the moiré patterns of defects in this two-dimensional array of domains and demonstrate that dislocations can be reliably imaged depending on the pitch of the moiré fringes and the orientation of the Burgers vector of the dislocations.

Introduction

Thin films of block copolymers are widely investigated for their potential uses in nanolithography, where the polymer film acts as a mask for etching nanometer-sized features. These systems are convenient because they self-assemble into periodic microdomains, and the size and periodicity of features can be tuned by changing the molecular weight and copolymer composition. A challenge that remains is controlling the long-range orientation of the microdomains and eliminating defects like dislocations that destroy translational periodicity. This is necessary for applications like high-density magnetic storage media, where the position of each storage unit must be known.[1] Alignment of block copolymer domains over micrometer length scales has been achieved with chemically patterned substrates, shear alignment, and graphoepitaxy.[2,3] Graphoepitaxy is a technique that uses topographically patterned substrates to laterally confine a single layer of the block copolymer domains over micrometer length scales, which are much larger than the periodicity of the individual microdomains.[4−6] In this work, we laterally confine a sphere-forming poly(styrene-*b*-2-vinylpyridine) block copolymer in hexagonal wells that match the rotational symmetry of the two-dimensional crystalline and hexatic phases of the microdomains. The hexagonal wells range in size from 2 to 100 μm across. We find that a single long-range orientation is templated in wells up to 12 μm across, where the close-packed rows are parallel to the confining edge, and the orientation of these grains in neighboring wells is the same.

Analysis of block copolymer grain structure across multimicrometer distances is a challenge due to the small size of the individual microdomains, which are typically on the order of 10−15 nm. Common analysis tools are scanning force microscopy (SFM) and scanning electron microscopy (SEM), but using SFM, resolution of the individual domains is only possible when small scan areas are employed ($1 \times 1\ \mu m^2$−$3 \times 3\ \mu m^2$ for the system described in this work), due to the finite sampling rate of 512 × 512 pixels per image of a typical SFM microscope. While SFM microscopes with higher sampling rates are available, the time to collect an image scales linearly with the number of pixels measured. As a result, it is difficult to determine the grain orientation and defect density of a monolayer confined in hexagons that are tens of micrometers across. In this work, we use a method first introduced by Angelescu et al.[7] to indirectly measure the grain structure and analyze the results based on the theory of moiré interference patterns.

Moiré patterns are formed from interference between a reference and a sample grating. Moiré analysis of grain structure was first demonstrated in electron microscopy, where two overlapping crystals were used to produce the interference patterns.[8−12] In SEM and SFM technologies, the raster motion itself builds a reference lattice of periodic scan lines.[13−15] In their pioneering experiments, Angelescu and co-workers[7] showed that SFM (and SEM) moiré patterns of spherical domain block copolymers arranged in a two-dimensional lattice could be obtained and analyzed. These authors developed an empirical calibration method to relate the angle and pitch of the moiré fringes to the block copolymer lattice orientation. The angle and pitch of the moiré patterns are highly sensitive to the grain orientation and lattice parameter of the underlying block copolymer sample. We demonstrate in this paper that SFM moiré patterns can be analyzed accurately using a simple analytical theory, obviating the need for a tedious empirical calibration. This theory can be applied to analyze block copolymers with different lattice parameters (e.g., different molecular weight). Under cer-

[†] Department of Materials, UC Santa Barbara.
[‡] Department of Chemical Engineering, UC Santa Barbara.
[§] Veeco Metrology.
* To whom correspondence should be addressed: e-mail edkramer@mrl.ucsb.edu; Tel (805) 893-4999.

10.1021/ma050286y CCC: $30.25
Published on Web 07/06/2005

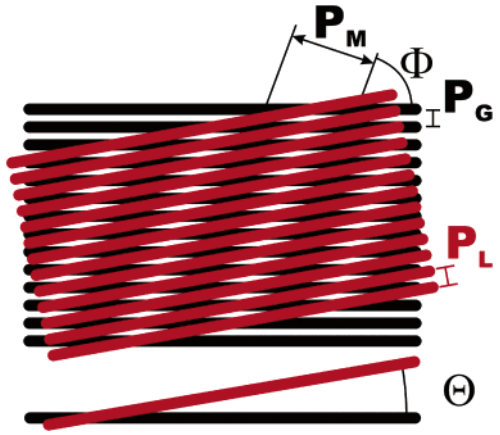

Figure 1. Moiré geometry: the relationship between Φ, Θ, P_M, P_G, and P_L.

tain conditions, we show that the patterns also reflect defects that disrupt translational and/or orientational periodicity in the lattice, such as dislocations and disclinations. Moiré analysis can therefore be used to ascertain the grain size, shape, orientation, and dislocation density, without resolving the individual spherical microdomains directly. This technique provides at a minimum a 10-fold increase in practical scan sizes without sacrificing time, so measuring the grain and defect structure across tens of micrometers is accomplished with a single measurement.

Moiré Analysis

The pitch and angle of the moiré patterns depend on the geometry of the block copolymer and reference lattices and can be related back to the sample lattice orientation and plane spacing with the following analytical equations derived from the system geometry, only two of which are independent.[13,14]

$$\frac{\sin(\Phi - \Theta)}{\sin(\Theta)} = \frac{nP_M}{P_G} \quad (1)$$

$$\frac{\sin(\Phi - \Theta)}{\sin(\Phi)} = \frac{nP_L}{P_G} \quad (2)$$

$$\frac{\sin(\Phi)}{\sin(\Theta)} = \frac{P_M}{P_L} \quad (3)$$

where n is an integer chosen such that $nP_L \approx P_G$. The other relevant parameters in eqs 1−3 for moiré analysis are the block copolymer lattice pitch P_L, the SFM grating pitch P_G, the moiré fringe pitch P_M, the lattice orientation angle Θ, and the moiré fringe orientation angle Φ, all of which are illustrated in Figure 1. For a 2D hexagonal system, the lattice pitch is the perpendicular distance between close-packed rows, or the {10} plane spacing, and Θ is the smallest angle between a close-packed row and the horizontal SFM scan axis. The moiré fringe angle Φ is likewise defined as the angle between the moiré fringe and the horizontal scan axis. The SFM grating pitch is the spacing between horizontal scan lines and is fixed by the ratio of scan size to image sampling rate (e.g., a 15 × 15 μm^2 SFM measurement at a sampling rate of 512 pixels has a grating pitch P_G = 15 μm/512 pixels). The grating pitch should be close to an integer multiple of the lattice pitch, $P_G \approx nP_L$, to avoid small pitch moiré fringes. The moiré pitch

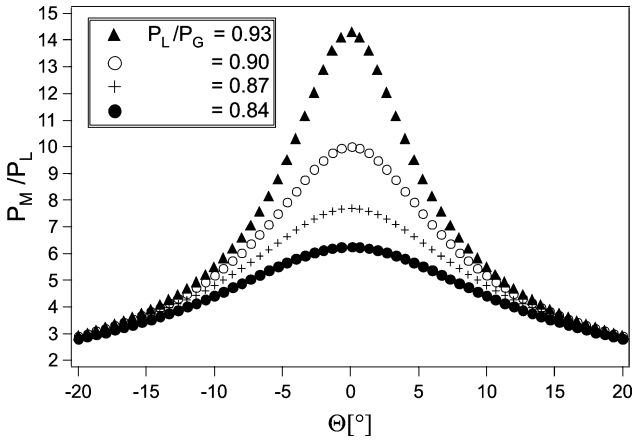

Figure 2. Moiré pitch P_M normalized by the lattice pitch P_L vs lattice orientation angle Θ calculated for different ratios P_L/P_G (n = 1).

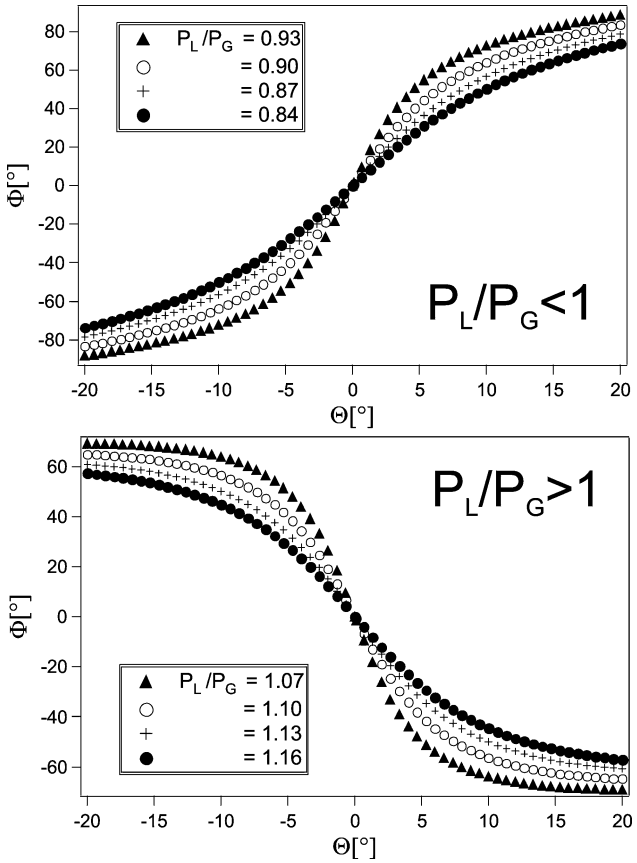

Figure 3. Moiré fringe angle Φ vs lattice orientation angle Θ calculated for different ratios P_L/P_G (n = 1).

P_M vs the lattice orientation angle Θ for several different P_L/P_G ratios is shown in Figure 2. Figure 3 shows the moiré fringe angle Φ as a function of Θ for values of P_L/P_G close to 1. When P_L/P_G < 1, Φ increases monotonically with Θ. If the grating pitch exactly matches the lattice pitch, eqs 1 and 2 are no longer valid. The upper limit for n is limited by the lattice pitch, the scan size of the SFM, and practical considerations like piezoelectric nonlinearities and drift of the SFM. A practical upper value in our experiments for n is 3 or a scan size of 45−50 μm.

Experimental Procedures

Synthesis. Poly(styrene-*b*-2-vinylpyridine) (PS−PVP) was synthesized via anionic polymerization as previously docu-

mented, resulting in a polydispersity index of 1.04, $N = 626$, and $f_{PVP} = 0.12$, where N is the total degree of polymerization of the block copolymer and f_{PVP} is the mole fraction of the PVP mers.[16] The PVP minority block forms spherical microdomains in a surrounding PS matrix. The thin film structure is a hexagonal lattice with a periodic nearest-neighbor spacing of 29 nm and a PVP core diameter of 9 nm.

Photolithography. A 25 nm thick layer of SiO_2 was deposited on a silicon wafer via plasma-enhanced chemical vapor deposition. A series of hexagons ranging in size from 2 to 100 μm across were patterned on the wafer with photolithography. This was followed by a dry etch (CHF_3 plasma) to produce 25 nm deep hexagonal wells in the exposed regions. After resist removal, the wafers were cleaned in piranha solution (H_2SO_4:H_2O_2 = 3:1, vol/vol) at 80 °C for 30 min to destroy any residual organic contamination. A 2 nm thick native oxide layer was allowed to regrow.

Sample Preparation. A 35 nm thick PS−PVP film was spun-cast on the patterned wafer from a 1 wt % toluene solution. The film thickness was selected to produce slightly underfilled wells, so excess material on the mesas between wells is drawn into the wells during the annealing. The result is a 20 nm polymer brush on the mesas and a 21 nm polymer monolayer plus 20 nm brush in the wells. Samples were annealed at 220 °C for 48 h under high vacuum (10^{-7} Torr) to prevent oxidation. Upon removal from the oven, samples were quenched below the glass transition temperature of both PS and PVP (100 °C) to freeze the structure. PS−PVP shows no SFM contrast after annealing because both PS and PVP have the same modulus, and the PS wetting layer at the top surface obscures the microstructure. An etch step to the midplane of the PVP cores is necessary for SFM analysis. The samples were etched with secondary ion mass spectrometry (SIMS) using the O_2^+ beam at a voltage of 1 kV, current of 25 nA, and raster size of 0.15 mm^2. Charge compensation was provided by a static 600 V electron beam. Negative ions of C^-, CN^-, and Si^- were monitored as a function of time, where the CN^- signal is unique to PVP. The SIMS etch was stopped just after a local maximum in the CN^- signal, indicating the location of the midplane of the spheres. The PVP etches slightly faster than the PS matrix, resulting in a 1 nm height difference between the PVP core and the PS matrix that can be measured with SFM.[4] The exposed PVP cores also show phase contrast in SFM from a stronger adhesive interaction with the tip.

Scanning Force Microscopy (SFM). All images presented here were taken with a Veeco Metrology Group Digital Instruments Dimension 5000 SFM. The SFM is mounted inside a temperature-controlled, vibration damped chamber to minimize thermal drift and noise. Both TESP and MPP-11200 tips by Nanodevices were used, both of which have a tip radius of ~10 nm and a spring constant of ~40 N/m. The SFM measures a sample with a raster-scan motion that consists of a fast (horizontal) and a slow (vertical) scan axis. Along the fast scan axis, data are collected every 16 μs and linearly averaged over the length of 1 pixel. The number of data points per pixel is therefore controlled by the scan rate and number of pixels per line (i.e., resolution). For a scan rate of 1 Hz, which refers to trace and retrace scans, at a resolution of 512 pixels, each pixel contains 64 measurements. The motion along the slow scan axis is achieved by repositioning the scanner by P_G at the start of each scan line. The image sizes for high-resolution scans, required for direct resolution of the spherical microdomains, are in the range 1×1 μm^2 to 2×2 μm^2 at a sample rate of 512×512 pixels per image. These images were taken under soft tapping conditions to optimize height contrast, running at a frequency of 1.1 Hz per scan line. The size of the moiré scans varied between 12×12 μm^2 and 15×15 μm^2. To achieve good phase contrast, the moiré images were taken under hard tapping conditions at a scan rate of 1.1 Hz. It is important to note that in moiré analysis the size of a pixel P_G is larger than the contact area of the tip with the sample, and therefore the measurement is undersampled.

Computation. The objectives of our analysis are to calculate the grain orientation angle Θ and the grain size from the moiré fringes. We chose to calculate Θ from eq 1 so that we do not need to specify the lattice pitch P_L, which is difficult to measure with high accuracy. Moiré patterns are visible in both the SFM height and phase images. The height contrast is a result of the selective etch previously described, and phase contrast is caused by the different adhesive properties of polystyrene and poly(styrene-*b*-2-vinylpyridine). Surface roughness adds noise to the height image, so it is preferable to use the phase image for analysis of the moiré patterns. The phase image does not require any image processing, so no artifacts are introduced by image manipulation.

Analysis of the moiré patterns is completed with a program coded in Visual Basic (Microsoft), using ImagePro Plus (Media Cybernetics) remotely via dynamic data exchange to compute the forward and inverse Fourier transforms. An example of a typical SFM phase image is shown in Figure 4a. The SFM phase image is first Fourier transformed with a fast Fourier transform (FFT) algorithm at a resolution of 512×512 points, resulting in Figure 4b. The FFT decouples the individual frequencies of the moiré patterns into distinct spectral peaks. The location of each Fourier peak is described by a vector $\vec{k} = (u, v)$ (Figure 4c) that corresponds with the pitch and angle of a specific moiré pattern in the real-space image. Therefore, the first step is to calculate the vector $\vec{k}$ from the FFT. The user provides an initial estimate of the peak coordinates (u, v) in pixels and then runs a center-of-mass routine that weights the Fourier amplitude over an 8×8 pixel square. The moiré fringe angle Φ is calculated from (u, v)

$$\Phi = \arctan\left(\frac{u}{v}\right) \tag{4}$$

The fringe pitch P_M (μm) is calculated from the magnitude of the Fourier vector $\vec{k}$ and the scan size L (μm)

$$P_M = \frac{L}{(u^2 + v^2)^{1/2}} \tag{5}$$

The grating pitch P_G (μm) is as previously defined, where r denotes the sampling rate along the slow scan axis

$$P_G = \frac{L}{r} \tag{6}$$

The lattice orientation angle Θ can now be calculated from Φ, P_M, and P_G by solving eq 1 for Θ

$$\Theta = \arctan\left[\frac{\sin(\Phi)}{\frac{nP_M}{P_G} + \cos(\Phi)}\right] \tag{7}$$

The image of every lattice grain is constructed by computing the inverse FFT for each individual Fourier peak with an 8×8 square kernel, where the coordinates (u, v) mark the center of the square. The 8×8 pixel square is chosen to preserve defects in the moiré pattern.[17] This produces a filtered real-space image for each Fourier peak (as illustrated in Figure 4d). The grain area is readily measured from the filtered image. The nonzero amplitudes in the inverse FFT are colored according to Θ and superimposed over the original SFM image for clarity.

Results and Discussion

Verification of the Moiré Analysis. The theoretical approach for analysis of moiré patterns is tested by imaging a spherical PS−PVP two-dimensional lattice confined laterally in a hexagonal well shown in Figure 5. The lattice is first imaged with a scan size of 2×2 μm^2 at a resolution of 512×512 pixels, which is sufficient to resolve each individual sphere as shown in Figure 5a. The lattice orientation angle is determined to be $0.5 \pm 1.7°$. The scan size is then increased to 12

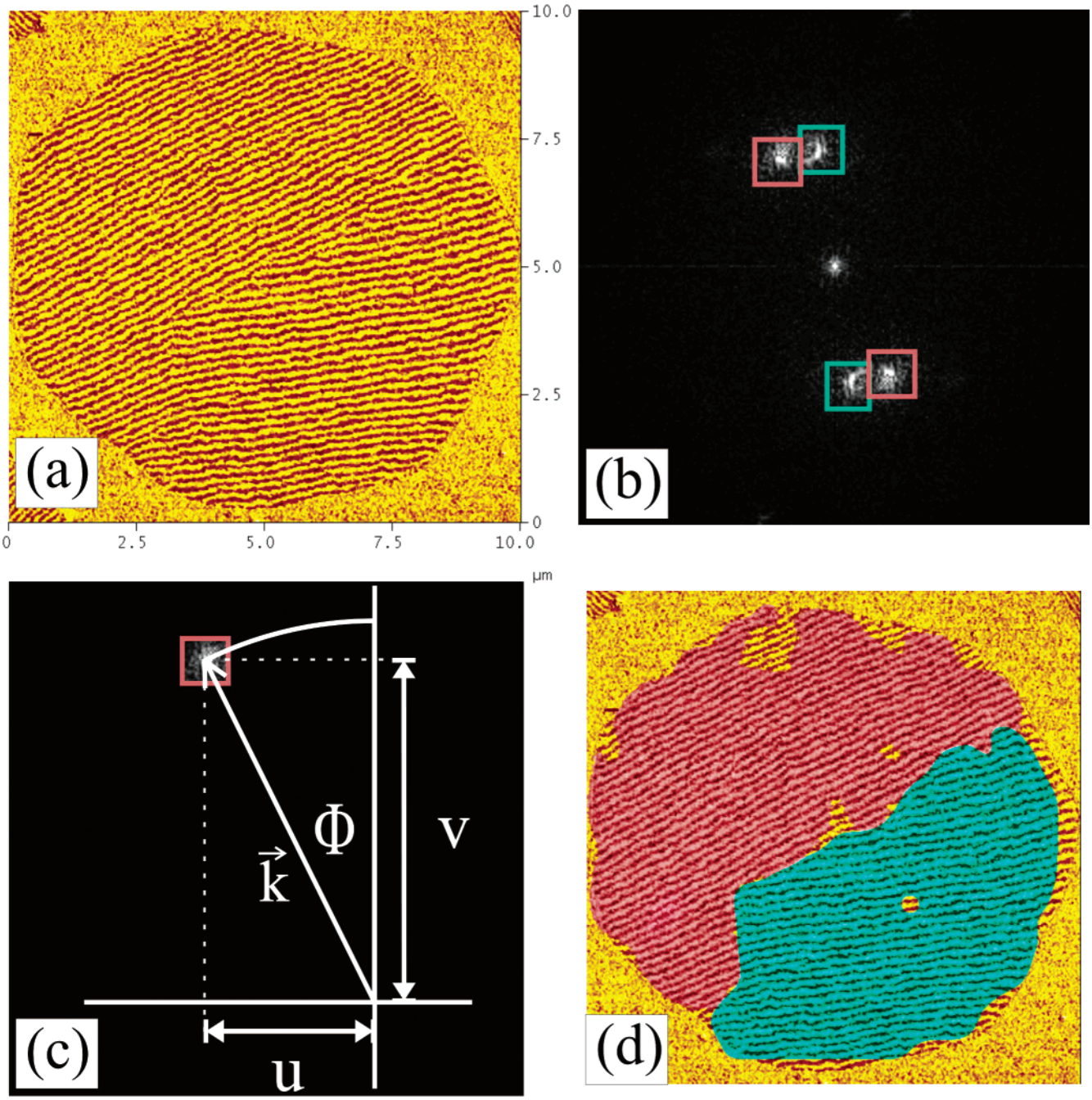

Figure 4. Analysis of moiré patterns: (a) shows moiré pattern of the block copolymer monolayer in a confined geometry. The fast Fourier transform is shown in (b). The pink and blue squares mark the Fourier peaks of interest. (c) defines the reciprocal lattice vector $\vec{k}$ of a set of moiré fringes and its components u and v. (d) shows the result where the two peaks in (b) are inverse Fourier transformed and overlaid with their respective color on the original image (a).

μm to form moiré patterns, and the sample is rotated from −19.5° to 20.5° in steps of 5°. The moiré patterns are analyzed as described in the previous section. The moiré fringe orientation angle Φ is determined using eq 4. The moiré pitch P_M is found using eq 5. The lattice orientation angle Θ is calculated at each scan rotation from Φ, P_M, and eq 7. The angles Φ and Θ calculated at each scan angle are fit to eq 2 using the lattice pitch as an adjustable parameter, shown in Figure 6. This fit yields a lattice pitch of 24.5 ± 0.2 nm, in excellent agreement with the pitch calculated from grazing-incidence small-angle X-ray scattering experiments on this block copolymer, which is 25 nm.

Moiré Patterns of Isolated Dislocations in 2D. The most common defects in a 2D array of spheres are disclinations, dislocations, and dislocation pairs. Lattice vacancies and interstitials are less prevalent. In a hexagonal lattice, every lattice point has six nearest neighbors arranged in a 6-fold symmetry. Disclinations are lattice site defects with 5 or 7 nearest neighbors. Removal of a −60° segment from a specific lattice point results in a −60° disclination, a site with only five nearest neighbors. Likewise, the insertion of a +60° segment in a 6-fold lattice site creates a +60° disclination, a site with seven nearest neighbors. The core of a dislocation is a pair of a 5-fold and a 7-fold disclination and marks the termination of two extra half-rows of spheres. The strength of a dislocation is measured by the Burgers vector, which is the extra step corresponding to a direct lattice vector in a loop that encloses the

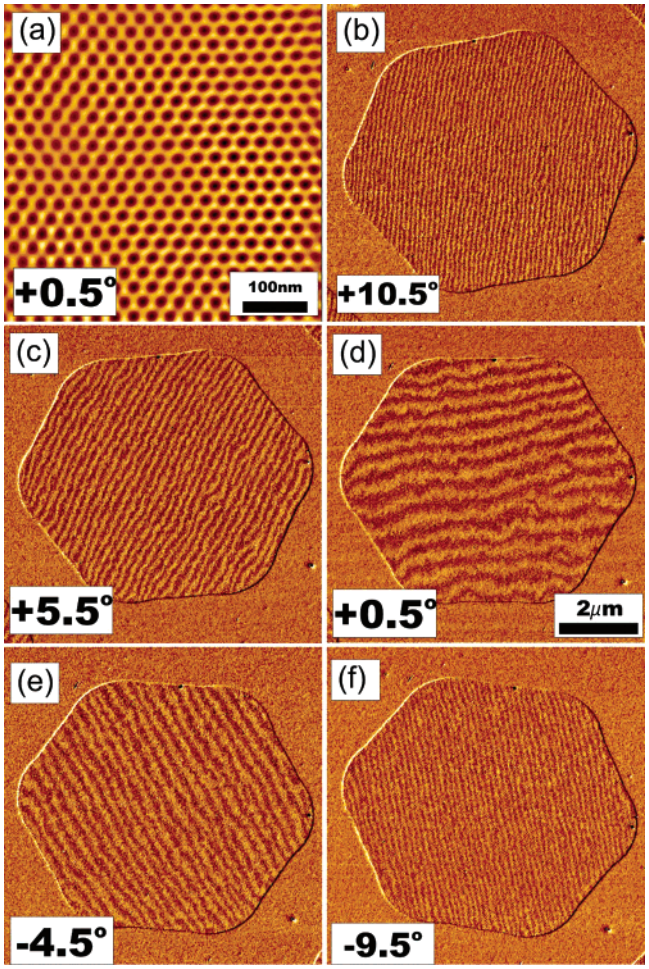

Figure 5. A hexagonal well 7 μm across is rotated from + 10.5° in (b) to −9.5° in (f). The grain orientation Θ is calculated at each scan angle. The image (a) is a Fourier filtered high-resolution image of the PS−PVP block copolymer lattice inside the hexagon for Θ = 0.5°.

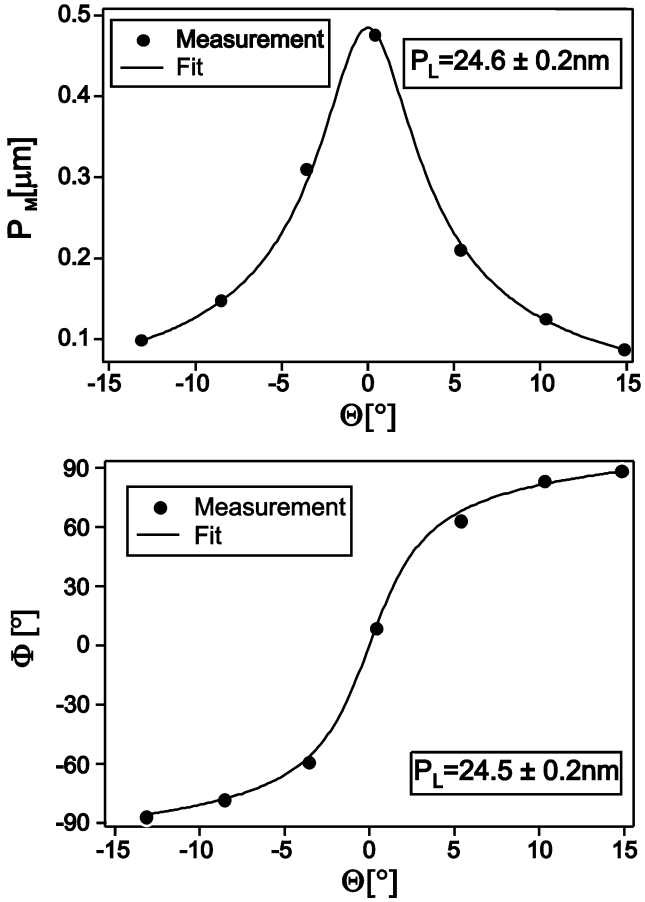

Figure 6. Top figure shows the measured moiré pitch P_M versus the lattice orientation angle Θ and the best fit to these data using the lattice pitch P_L. The lower figure shows the measured moiré angle Φ versus Θ and the best fit to these data using the lattice pitch P_L as an adjustable parameter. The value of P_L for best fit is shown in both figures.

dislocation core.[18] Two dislocations can form a close dislocation pair, separated by one lattice spacing, if they have opposite Burgers vectors.[19] These dislocation pairs, or disclination quadrapoles since they consist of four disclinations, have zero net Burgers vector. Under certain conditions, moiré interference can detect isolated dislocations and disclinations because only these defects destroy the translational periodicity over a long range. In general, isolated disclinations are only present in the two-dimensional liquid. Moiré interference requires a regular lattice, so we restrict the following discussion to detection of dislocations.

In the moiré pattern, an extra half row of spheres from a isolated dislocation is characterized by the termination of a fringe.[9] The criteria for observing dislocation fringes are related to the lattice orientation and the moiré pitch. The close-packed row that forms the lowest angle with the scan direction, denoted earlier by Θ, is the direction that produces the strongest fringes. There are three such directions in the hexagonal lattice because with 6-fold symmetry there are three mirror planes (i.e., Θ and Θ ± 60°). To see a dislocation, one of the inserted half rows must be along the close-packed row that forms the smallest angle with the scan direction; otherwise, there is no disruption in the translational periodicity of the lattice grating. Out of six possible orientations for the Burgers vector, only four will be associated with inserted half rows parallel to the scan direction. A reciprocal lattice vector $\vec{q}_\Theta$ is introduced to describe the lattice grating of close-packed rows forming an angle Θ with the scan direction, and $\vec{b}$ denotes the Burgers vector of the dislocation. The condition

$$\vec{q}_\Theta \cdot \vec{b} \neq 0 \tag{8}$$

must be fulfilled if the dislocation is to be visible in the moiré fringe pattern. On average only two-thirds of all dislocations will satisfy eq 8 for any given Θ, so it is necessary to rotate the sample (or, equivalently, the scan direction) to scan at Θ, Θ + 60°, and Θ − 60° in order to detect all isolated dislocations and determine their Burgers vectors $\vec{b}$ by their disappearance when $\vec{q}_\Theta \cdot \vec{b} = 0$.

It is important to note that this technique is best suited for low dislocation densities, where the distance separating single dislocations with opposite Burgers vectors is greater than the pitch of the moiré fringes. When this condition is not satisfied, inserted fringes, corresponding to the underlying dislocations, which overlap along the fast scan axis and are separated along the slow scan axis by less than the moiré pitch, merge into one fringe, and can no longer be distinguished.

Figure 7 shows a high-resolution SFM image of three dislocations, overlaid with the Voronoi construction calculated from the position of each sphere. Two inserted half rows for every dislocation are marked in

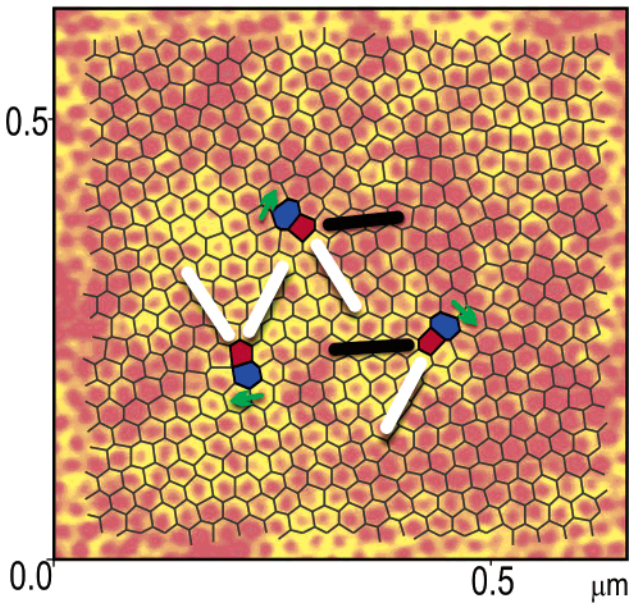

Figure 7. High-resolution SFM image, overlaid with the Voronoi construction[20] calculated from the position of each sphere. Two inserted half rows for every dislocation are shown in white and black and the corresponding Burgers vector of each dislocation in green.

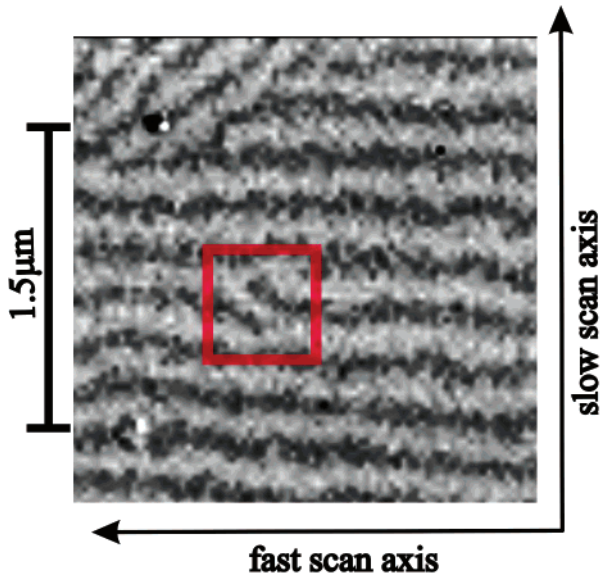

Figure 8. Moiré scanning microscope image of a small selected region surrounding the defects shown in Figure 7 from a much larger 15.4 μm × 15.4 μm moire scan with a ratio of lattice pitch to scanning pitch = 0.83. The red square marks the area shown in Figure 7.

white or black and the corresponding Burgers vector of each dislocation in green. The half rows marked in black produce the inserted moiré fringes. Of the three dislocations, one has a Burgers vector parallel to the fast scan axis and therefore fails the condition set by eq 8. The other dislocations have Burgers vectors rotated ±120° and are observed in the moiré pattern shown in Figure 8. In Figure 9, the ratio of lattice pitch to grating pitch is close to unity (P_L/P_G = 0.93), so the moiré pitch approaches a value larger than the distance between the two visible defects in Figure 8. Therefore, the dislocations visible in the moiré pattern of Figure 8 can no longer be detected. The red box in Figures 8 and 9 outlines the area of Figure 7.

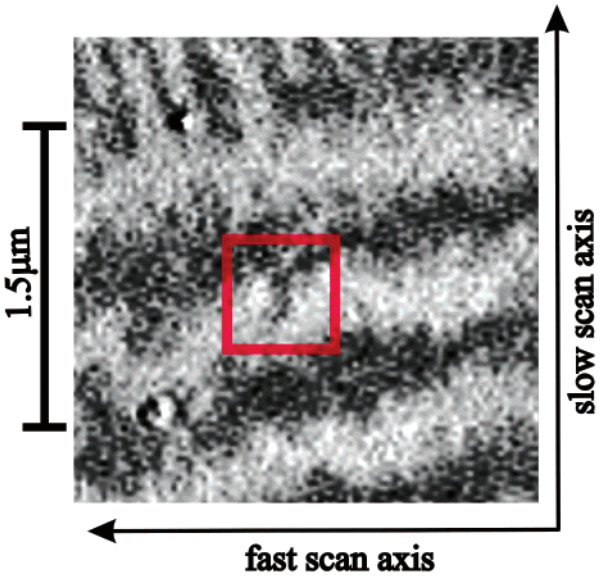

Figure 9. Moiré scanning microscope image of a small selected region surrounding the defects shown in Figure 7 from a much larger 13.1 μm × 13.1 μm moire scan with a ratio of lattice pitch to scanning pitch = 0.98. The red square marks the area shown in Figure 7.

Conclusions

We have outlined the conditions necessary for producing moiré patterns from interference between SFM scan lines and a two-dimensional spherical block copolymer lattice. We demonstrate that the periodicity and angle of the moiré patterns are related analytically to the orientation, grain size, and plane spacing of the block copolymer lattice. The conditions for detecting single dislocations with moiré interference and calculation of their Burgers vectors are described. This technique is a simple route to increase the scan area 2 orders of magnitude, providing a drastic improvement in statistics without sacrificing measurement time. The technique and analysis are relevant to a wide range of systems extending beyond block copolymers, including any pattern with nanoscale periodicity that can be measured with SFM or SEM technologies.

Acknowledgment. This work was supported by the National Science Foundation-DMR-Polymers Program Award No. DMR0307233 and benefited from the use of the MRL Central Facilities supported by the NSF MRSEC Program under Award No. DMR00-80034.

References and Notes

(1) Naito, K.; Hieda, H.; Sakurai, M.; Kamata, Y.; Asakawa, K. *IEEE Trans. Magn.* **2002**, *38*, 1949.
(2) Hamley, I. W. *Nanotechnology* **2003**, *14*, R39−R54.
(3) Park, C.; Yoon, J.; Thomas, E. L. *Polymer* **2003**, *44*, 6725.
(4) Segalman, R. A.; Yokoyama, H.; Kramer, E. J. *Adv. Mater.* **2001**, *13*, 1152.
(5) Cheng, J. Y.; Ross, C. A.; Thomas, E. L.; Smith, H. I.; Vancso, G. J. *Appl. Phys. Lett.* **2002**, *81*, 3657.
(6) Sundrani, D.; Darling, S. B.; Sibener, S. J. *Nano Lett.* **2004**, *4*, 273.
(7) Angelescu, D. E.; Harrison, C. K.; Trawick, M. L.; Chaikin, P. M.; Register, R. A.; Adamson, D. H. *Appl. Phys. A* **2004**, *78*, 387.
(8) Dowell, W. C. T.; Farrant, J. L.; Rees, A. L. G. *1957 Proc. Regional Conf. Electron Microsc., Tokyo* **1956**, 320.
(9) Pashley, D. W.; Menter, J. W.; Basset, G. A. *Nature (London)* **1957**, *179*, 752.
(10) Hashimoto, H.; Uyeda, R. *Acta Crystallogr.* **1957**, *10*, 1431.

(11) Read, D. T.; Dally, J. W. *J. Res. Natl. Inst. Stand. Technol.* **1996**, *101*, 47.
(12) Bassett, G. A.; Menter, J. W.; Pashley, D. W. *Proc. R. Soc. London A* **1958**, *246*, 345.
(13) Lu, Y. G.; Zhong, Z. W.; Yu, J.; Xie, H. M.; Ngoi, B. K. A.; Chai, G. B.; Asundi, A. *Rev. Sci. Instrum.* **2001**, *72*, 2180.
(14) Chen, H.; Liu, D.; Lee, A. *Exp. Technol.* **2000**, *24*, 31.
(15) Whangbo, M. H.; Liang, W.; Ren, J.; Magonov, S. N.; Wawkuschewski, A. *J. Phys. Chem.* **1994**, *98*, 7602.
(16) Yokoyama, H.; Mates, T. E.; Kramer, E. J. *Macromolecules* **2000**, *33*, 1888.
(17) Pradere, P.; Thomas, E. L. *Ultramicroscopy* **1990**, *32*, 149.
(18) Chaikin, P. M.; Lubensky, T. C. In *Principles of Condensed Matter Physics*; Paperback; Cambridge University Press: Cambridge, 2000; p 663.
(19) Segalman, R. A.; Hexemer, A.; Hayward, R. C.; Kramer, E. J. *Macromolecules* **2003**, *36*, 3272.
(20) Voronoi, G. F. *J. Reine Angew. Math.* **1909**, *136*, 67.

MA050286Y